RSC Advances

ROYAL SOCIETY OF CHEMISTRY

www.rsc.org/advances

Journal Name

ARTICLE

MnO₂ nanosheets as a high-efficiency electrocatalyst for H_2O_2 reduction in alkaline medium

Zhuang Cai[a,b], Dongming Zhang[a], Liangliang Gu[a], Ping Liu[c*], Ke Ye[a], Kui Cheng[a], Dianxue Cao[a], Guiling Wang[a*]

Considering the good ability of MnO₂ on the breakage of HO-OH bond in H₂O₂, we employed C@TiO₂ nanowires supported MnO₂ as a novel catalyst for H₂O₂ electroreduction. The morphology and phase structure of the MnO₂/C@TiO₂ electrode are characterized by scanning electron microscopy, transmission electron microscopy and X-ray diffractometer. The catalytic activity of the MnO₂/C@TiO₂ electrode for H₂O₂ electroreduction is investigated by means of cyclic voltammetry and chronoamperometry. The catalyst exhibits a high catalytic activity and good stability in the electrochemical reaction process. The oxidation current density is higher than 200 mA cm⁻² at -0.7 V in 1.6 mol dm⁻³ H₂O₂. The popular price, abundant reserves, promising electrocatalytic performance make it a viable catalyst for H₂O₂ electroreduction.

1. Introduction

Fuel cells (FCs), a device directly converting chemical energy of a fuel into electrical energy, are highly desirable with the depletion of fossil fuels and the ever increasing demands for clean energy [1-3]. Compared with lithium batteries, FCs have intrinsic advantages in power density and energy supply, which make them promising practical in spaceships [4], underwater [5], hybrid vehicles [6] energy supplying devices and so on. Hydrogen peroxide (H₂O₂) has been seen as a viable oxidizer for liquid-based FCs, such as metal semi-FCs [7-8], direct borohydride–hydrogen peroxide FCs [9-14], direct peroxide–peroxide FCs [15-16], direct methanol–hydrogen peroxide FCs and so on [17-18]. The electroreduction towards H₂O₂ in cathode is a two-electron transfer process involving the breakage of single dioxygen bonds (Eq. 1) [7-32] with a standard electrode potential of 0.878 V, leading a lower reaction active-energy compared with the O₂ electroreduction of the double of single dioxygen bonds (Eq. 2) [33-39] and higher cathode potential (0.401 V). Besides, the H₂O₂ is liquid, which establish a simple solid-liquid two-phase reaction and is easy to construct a more stable, compact and convenient FC system [7-18]. So FCs employing H₂O₂ as oxidant with high performance may be potential electrochemical devices to replace O₂ in some operational places without oxygen, such as space station, submarine and so on.

$$H_2O_2 + 2e^- \rightarrow 2OH^- \qquad E^0 = 0.878 \qquad (1)$$

$$O_2 + 2H_2O + 4e^- \rightarrow 4OH^- \qquad E^0 = 0.401 \qquad (2)$$

The design of cathode catalysts with excellent electrocatalytic activity for H₂O₂ reduction is one of the decisive factors that determine the performance of FCs. In general, precious metals, such as Pt [19-20], Pd [21], Au [22] and their alloys, are considered as the best catalysts for various electrocatalytic reactions due to their superior ability to trap electrons. However, the use of noble metals is limited by their scarcity and high cost, which give impetus to the attention on the inexpensive choices to supersede noble metals.

Currently, macrocycle complexes of transition metals, such as Fe- and Co- porphyrin [23-25], transition metal and their oxides, such as cobalt [21], copper oxides [26], cobalt oxides [27-31], ferric oxides [32], perovskite-type oxides [14] are studied as low cost catalysts and alternative to noble metals for H₂O₂ eletroreduction. Lei et al. [31] reported an aligned Co₃O₄ nano-walls electrode as the H₂O₂ sensor based on the electrocatalytic oxidation and reduction of H₂O₂. A fast response and high sensitivity were successfully obtained at applied potentials of +0.8 V and -0.2 V (vs. Ag/AgCl). Our team [26] previously prepared a Cu foil based CuO nanosheets through a simple chemical oxidation process. The low-cost, abundant resource and easy preparation of CuO/Cu made it a promising electrode for FCs using H₂O₂ as oxidants.

MnO₂, as a cost-effective and important electrochemical material, has been widely used in lithium batteries [40-41], supercapacitors [42-43], FCs [44-45], electrochemical sensors [46-47] and so on. For example, owning to its high specific

[a.] Key Laboratory of Superlight Materials and Surface Technology of Ministry of Education, College of Materials Science and Chemical Engineering. Harbin Engineering University, Harbin, 150001, P.R.China.E-mail: wangguiling@hrbeu.edu.cn; Fax: +010-86-451-82589036; Tel: +010-86-451-82589036.
[b.] Key Laboratory of Functional Inorganic Material Chemistry, Ministry of Education, School of Chemistry and Materials Science, Heilongjiang University, Harbin, 150080, P. R. China.
[c] Beijing Center for Diseases Prevention and Control, Beijing, 100013, P.R.China.E-mail: Cissy0511@126.com.

capacitance, low cost, natural abundance, and environmental benignity, MnO_2 is regarded as the most practical stuff in the field of electrochemical energy storage. Moreover, MnO_2 can efficaciously break O-O bond in HO_2^- and catalytic HO_2^- disproportionation (Eq.3 and 4) [33-35] and receives intensively interests on the FCs (Employing O_2 as oxidizer), metal/air (O_2) batteries, electrochemical sensors (H_2O_2) [33-35, 45, 47]. However, to the best of our knowledge, few of report applied MnO_2 for H_2O_2 electrochemical reduction in fuel cells.

$$HO_2^- + 2H_2O + 2e^- \rightarrow 3OH^- \qquad (3)$$

$$2HO_2^- \rightarrow 2OH^- + O_2 \qquad (4)$$

In this paper, we use a $C@TiO_2$ nanowire based MnO_2 nanosheets [42] as an active and stable catalyst for H_2O_2 electroreduction. The $C@TiO_2$ nanowire were prepared by a simple chemical vaporous deposition (CVD) using Ti foil as substrate and acetone as carbon source and following a electrodeposition process to deposit MnO_2. This $MnO_2/C@TiO_2$ electrode owns a unique three dimensional (3D) porous structure, which is facile for the diffusion of H_2O_2 and the release of O_2 during the reaction process (Eq. 4). The $MnO_2/C@TiO_2$ achieved an open circle potential of -0.2 V and a reduction current density of 200 mA cm^{-2} at -0.7 V in a solution containing 3 mol dm^{-3} NaOH and 1.6 mol dm^{-3} H_2O_2.

2. Experimental

2.1. Reagents

Acetone (CH_3COCH_3), isopropanol (($CH_3)_2CHOH$), ethanol (C_2H_5OH), hydrofluoric acid (HF), nitric acid (HNO_3), manganese acetate ($MnAc_2$), ammonium acetate (NH_4Ac), dimethyl sulfoxide (DMSO), sodium hydroxide (NaOH), hydrogen peroxide (H_2O_2) were obtained from Enterprise Group Chemicals Reagent Co. Ltd. China. Ar gas was gotten from Liming Gas Co. Ltd. Ti foil was purchased from Baoji Yiyuan titanium industry Co., Ltd. All chemicals are analytical grade and were used as-received without further purification. Ultra-pure water (Millipore, 18 MU cm) was used throughout the study.

2.2. Preparation and characterization of $MnO_2/C@TiO_2$

The synthesis of $MnO_2/C@TiO_2$ is shown by Fig. 1. The $C@TiO_2$ substrate was first prepared by a Huo's method [48]. Briefly, Ti foil (10× 10 × 1 mm^3 sizes, 1 cm^2 planar area) were degreased ultrasonically in acetone, isopropanol and ethanol sequentially for 15 minutes, then polished with a solution containing H_2O, HNO_3 and HF with a volume ratio of 5:4:1 for 5 minutes. Following, the Ti foil were loaded onto a ceramic substrate and put into the center of a horizontal tube furnace after rinsing with deionized water. Before being heated to 850 ℃ under argon, the tube furnace was purged with argon several times. Acetone was introduced into the tube furnace by argon at a flow rate of 150 SCCM (SCCM represents standard cubic centimeter per minute at STP) for 1.5 h under 850 ℃. C/TiO_2 nanowires were obtained after they were cooled to room

temperature under argon. During this process, carbon-containing and oxygen-containing species including • CH_3 radicals and CO were produced first by the thermal decomposition of CH_3COCH_3. Then, Ti atoms on the surface of Ti foil will adsorb and reacts with the as-generated CO to form TiO_2 and C ($Ti + 2CO \rightarrow TiO_2 + C$). Notably, TiO_2 nanowires shaped with the diffusion of Ti atoms upwards along the formed TiO_2 and • CH_3 also took part in the formation of C, as described by Huo's work [48].

Then, MnO_2 nanosheets were coated on the as-prepared $C@TiO_2$ through one step electrodeposition process as our previous report [42]. The C/TiO_2 nanowires were used as working electrode, a carbon rod (3 mm in diameter) was served as counter electrode, and a saturated Ag/AgCl, KCl electrode was used as reference electrode. Anodic electrodeposition of MnO_2 nanoplates were performed at a constant current of 1 mA cm^{-2} for 5 minutes in a solution contained 0.01 mol dm^{-3} manganese acetate ($MnAc_2$) and 0.02 mol dm^{-3} ammonium acetate (NH_4Ac) and 10% dimethyl sulfoxide (DMSO) at 70 ℃ in a typical three-electrode electrochemistry cell with glass cell with an electrochemical station (CHI660D).

H_2O_2 electroreduction was also performed in the same three-electrode electrochemical cell using the 1 cm^2 $MnO_2/C@TiO_2$ electrode. All potentials were referred to the saturated Ag/AgCl, KCl reference electrode. The morphology of the electrodes was determined using a scanning electron microscope (SEM, JEOL JSM-6480) and transmission electron microscope (TEM, FEI TeccaiG2S-Twin, Philips). The structure was analyzed by a powder X-ray diffractometer (XRD, Rigaku TTR-III) equipped with Cu Kαradiation (λ= 0.15406 nm).
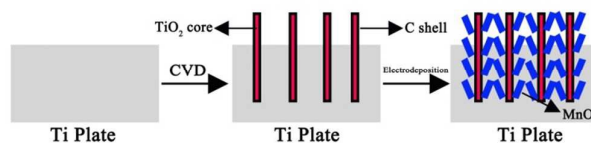

Fig. 1 Fabrication process of $MnO_2/C@TiO_2$ electrode.

3. Results and discussion

MnO_2 nanoplates were deposited on the $C@TiO_2$ via an electrodeposition process, in which the electrodeposition time was used to play an important role in both surface morphology and electrocatalytic performance. Fig.2 shows the SEM images of $C@TiO_2$ substrate and $MnO_2/C@TiO_2$ (b ~ f) with different electrodeposition time (10~120 min), insert in (d) is the TEM image of the single $MnO_2/C@TiO_2$ nanowire. After the chemical vapor deposition (CVD), aligned nano-needles with smooth face and about 500~600 nm length were observed uniformly distributed on the Ti foil surface (Fig. 2a) and formed a three dimensional (3D) open porous structure, which is favorable for the electrolyte diffusion [42] and MnO_2 deposition. The subsequent electrodeposition process make MnO_2 equally coated around the $C@TiO_2$ nanowires. Interestingly, the MnO_2 exhibits nanoplate-like structure

rather than nanoparticles, leading more catalytic sites and ensures closely contact between reactant and catalyst. The loading of MnO_2 increases with increase the electrodeposition time (Fig. 2b~f). When the time is 10, 30 and 60 min, we can see both of the $C@TiO_2$ wires and MnO_2 plates. The $C@TiO_2$ wires were completely covered by MnO_2 and disappeared in our vision field with the time reached to 90 and 120 min. TEM image was employed to gain further insights of the $MnO_2/C@TiO_2$ (Insert in Fig. 2d). Clearly, the length and width of $C@TiO_2$ are 600 and 200 nm, respectively, with a 30 nm thickness of carbon shell. MnO_2 nanoplates were observed in the carbon surface, which is consistent with the SEM result. The crystallographic property was analyzed by X-ray diffraction and shown in Fig. 3. There are three kinds of characteristic peaks assigned to Ti (JCPDS card: 44-1294), TiO_2 (JCPDS card: 21-1276) and MnO_2 with unknown structure (12-0141) [42-43], respectively, during scan range of 15° to 80°.
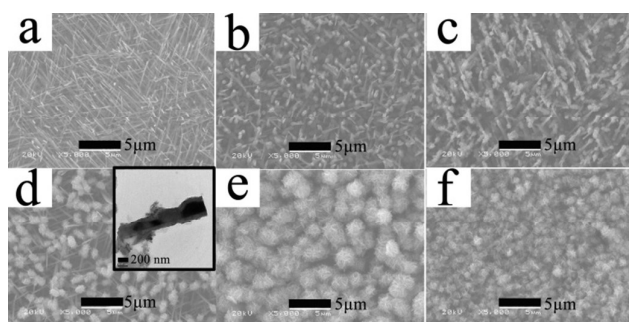

Fig. 2 SEM images of $C@TiO_2$ substrate (a) and $MnO_2/C@TiO_2$ (b ~ f) with different electrodeposition time (10~120 min), insert in (d) is TEM image of the single $MnO_2/C@TiO_2$ nanowire.

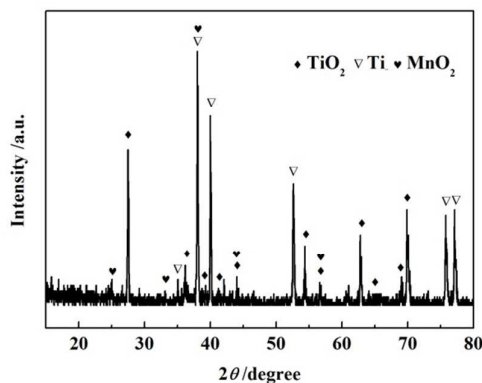Fig. 3 XRD patterns of $MnO_2/C@TiO_2$ electrode.

XPS measurement was investigated to further analyze the surface composition of $MnO_2/C@TiO_2$ and the result was shown in Fig. 4. The survey scan indicated the presence of Mn, O, C and Ti in the electrode. Insert in Fig. 4 is the high resolution XPS data for Mn 2p, presenting two peaks at 641.6 and 653.3 eV owning to the binding energy of Mn 2p3/2 and Mn 2p1/2, respectively, from the Mn^{4+} (MnO_2).

Cyclic voltammetry (CV) curve is engaged to assess the electrocatalytic performance of $MnO_2/C@TiO_2$ electrode in H_2O_2 solution. We first investigate the effect of electrodeposition time on the electrocatalytic activity of $MnO_2/C@TiO_2$ for H_2O_2 reduction and the results are shown by Fig. 5. We can see that the reduction current densities seriously depend on the MnO_2 loading and the $C@TiO_2$ substrate almost exhibits no electrocatalytic performance for H_2O_2 reduction, demonstrating that the C coated TiO_2 only serves as supporter for the loading of MnO_2, which will play the role of an efficient catalyst for H_2O_2 electroreduction. The current density first increased remarkably with the increase of electrodeposition time and reached to 180 mA cm^{-2} at -0.7 V when the time rises to 60 min, demonstrating that extending electrodeposition can obviously improve the catalytic properties of $MnO_2/C@TiO_2$. However, when the time is longer than 60 min, the current density decreased from 180 to 60 mA cm^{-2}, respectively, in response to 90 and 120 min. Clearly, the MnO_2 prepared with 60 min shows the best performance among these samples. Besides, a weak reduction peak, involved to the electroreduction of H_2O_2 (Eq. 1) [7-32], centered at around -0.62 V, when the electrodeposition times are fixed at 10, 30 and 120 min and this phenomenon only occurred at the electrode with low efficiency. As shown in Fig. 2, the MnO_2 loading is insufficient in short electrodeposition time (10 and 30 min) and superfluous in long electrodeposition time (90 and 120 min), the first situation will not provide competent active sites to contact with oxidant and the other may block up the 3D porous structure and the oxygen can't be released soon, both of which will lead a damping for H_2O_2 reduction. Besides, manganese oxides are semiconducting materials, increasing the amount of MnO_2 will weaken the electric conductivity and further reduce the catalytic activity.
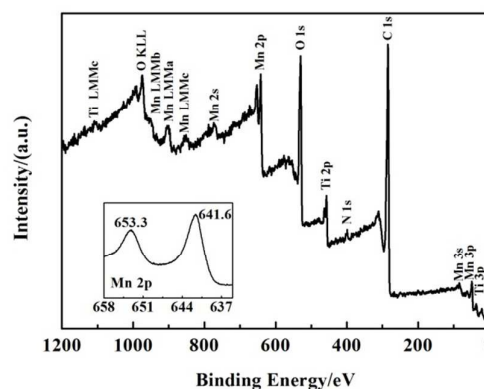

Fig. 4 XPS survey scan spectra of $MnO_2/C@TiO_2$ (Insert is the high resolution XPS data for Mn 2p).

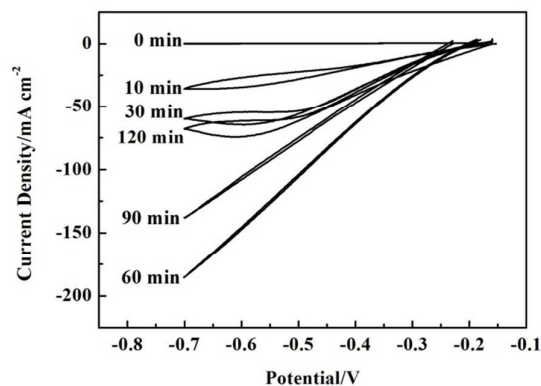Fig. 5 Cyclic voltammetry (CV, Scan rate: 5 mV s^{-1}) curve of MnO$_2$/C@TiO$_2$ with different electrodeposition time (0~120 min) in 3 mol dm^{-3} NaOH and 1.2 mol dm^{-3} H$_2$O$_2$.

OH$^-$ plays an important role in the whole reaction process (Eq. 1~4) [7-39] and it is significative to discuss the effect of NaOH concentration on the electrochemical performance. Fig. 6a presents the CVs of MnO$_2$/C@TiO$_2$ electrode in different concentrations of NaOH (1~4 mol dm^{-3}) with H$_2$O$_2$ concentration constantly kept at 1.2 mol dm^{-3}. It can be observed that the reduction current density of MnO$_2$/C@TiO$_2$ increased with the increase of NaOH concentration from 1 to 3 mol dm^{-3} and slightly decreased with the further increase to 4 mol dm^{-3}. So 3 mol dm^{-3} NaOH gives the best performance when the H$_2$O$_2$ concentration is 1.2 mol dm^{-3} and demonstrate that the optimal electrochemical performance only occurs within suitable ration of [OH$^-$/H$_2$O$_2$] (around 2) rather than immensely raise or reduce alkaline concentration.
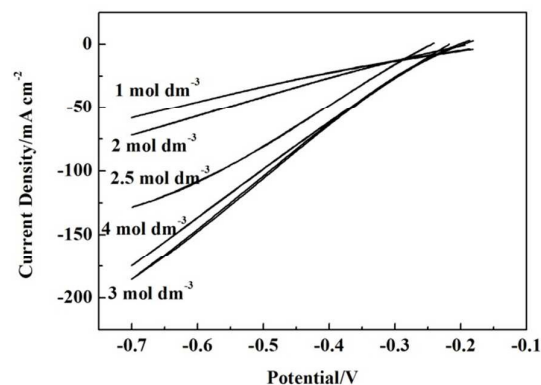

Fig. 6 CVs (a, Scan rate: 5 mV s^{-1}) of MnO$_2$/C@TiO$_2$ (60 min) in 1.2 mol dm^{-3} H$_2$O$_2$+x (x=1, 2, 2.5, 3, 4) mol dm^{-3} NaOH.

The effects of H$_2$O$_2$ concentration on the catalytic behavior of MnO$_2$/C@TiO$_2$ were investigated and the results are shown in Fig. 7. Similar as the Fig. 5, a weak reduction peak emerged in the CV curves (Fig. 7) with low catalytic performance and the current density increased with the increase of H$_2$O$_2$ concentration, manifesting the reaction was controlled by

diffusion. The increasement tendency of reduction current density between the H$_2$O$_2$ concentration of 1.2 and 1.6 mol dm^{-3} decreased abruptly demonstrated that the current density isn't in proportion to the fuel concentration. The conclusion is in point to the NaOH concentration at the same time. Besides, it must be pointed that the bare C@TiO$_2$ substrate almost has no catalytic activity for H$_2$O$_2$ reduction. Although the catalytic activity of MnO$_2$/C@TiO$_2$ for H$_2$O$_2$ reduction can't be comparable to the previous noble metals and some our prior Co$_3$O$_4$, Co$_x$Mn$_y$O, NiCo$_2$O$_4$ electrodes [27-30], it is still a potential electrode due to its low cost and rich deposits.
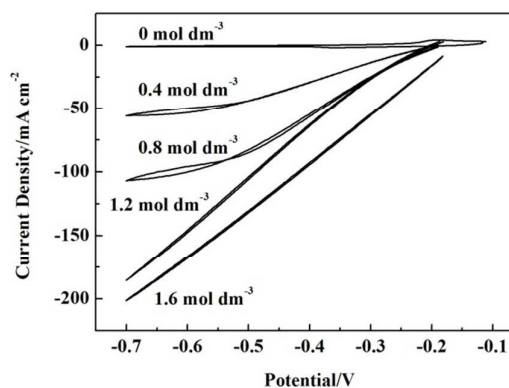

Fig. 7 CVs (a, Scan rate: 5 mV s^{-1}) of MnO$_2$/C@TiO$_2$ (60 min) in 3 mol dm^{-3} NaOH +x (x=0, 0.4, 0.8, 1.2, 1.6) mol dm^{-3} H$_2$O$_2$.

The catalytic activity of MnO$_2$/C@TiO$_2$ for H$_2$O$_2$ electroreduction was further tested by changing the reaction temperature in a solution containing 3 mol dm^{-3} NaOH and 1.2 mol dm^{-3} H$_2$O$_2$, and the result was recorded in Fig. 8. Higher temperature will lead faster electrode kinetics [21] and accelerate H$_2$O$_2$ reaction speed on MnO$_2$ surface. Under this circumstance, more HO-OH bonds were broken, resulting in the increasing of reduction current density (From 303.15 to 333.15 K). Unfortunately, over high temperature cause a critical hydrolysis of H$_2$O$_2$ [21, 49], which will reduce the utilization of fuel and may destruct the electrode structure. As a consequence, the catalytic performances rapidly fall off when the reaction was conducted at 343.15 and 353.15 K.
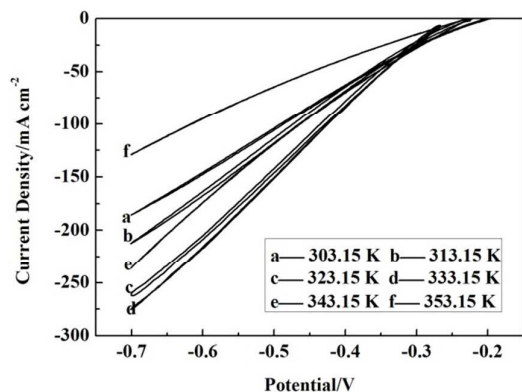
ARTICLE

Fig. 8 CVs (Scan rate: 5 mV s^{-1}) of MnO$_2$/C@TiO$_2$ (60 min) in 3 NaOH mol dm^{-3} +1.2 mol dm^{-3} H$_2$O$_2$ at different temprature (303.15~353.15 K).
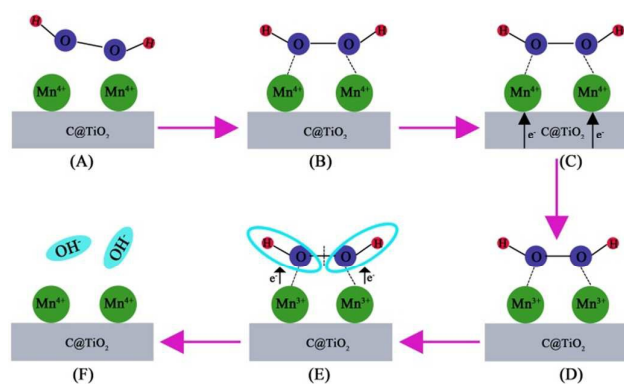

Fig. 9 Schematic diagram depicting the mechanism for the H$_2$O$_2$ electroreduction on the MnO$_2$/C@TiO$_2$.

The highest current density reached up to 175 mA cm^{-2} at -0.7 V in 1.2 mol dm^{-3} H$_2$O$_2$ at 303.15 K (Fig. 7a), which is much higher than our previous Cu based CuO electrode [26]. The good electrocatalytic activity can be attributed to the following three reasons: First, the MnO$_2$/C@TiO$_2$ owns a unique 3D porous structure and provide an excellent electronic conductivity; second, the MnO$_2$ nanoplates uniformly coated on the C/TiO$_2$ surface, instead agglomeration as some other electrode prepared through slurry and coating with binders; last and the most important, according to the previous reports [33-35], MnO$_2$ has fine ability to break the HO-OH bond during the reaction, which is the essential factor to drive the occurance of H$_2$O$_2$ electroreduction. As seen from Fig. 9, the atomic oxygen may be firstly adsorbed on the MnO$_2$ (Mn^{4+}) surface (Fig. 9 A→B) due to its weak electronegativity in H$_2$O$_2$. Then MnO$_2$ absorbs some electrons, transported from external circuit, and transformed to Mn^{3+} (C→D). Mn ion has a laigh electron affinity, so the Mn^{3+} will release the electron, mentioned in (C→D), to the adsorbed H$_2$O$_2$ molecule (E). At last, the HO-OH bond was broken after obtain electrons and formed OH- (C→D). Synchronously, Mn^{3+} returns to Mn^{4+} (MnO$_2$).

The stability of MnO$_2$/C@TiO$_2$ for H$_2$O$_2$ electroreduction at different applied potential was performed by CA test. The potential ranges from -0.6 to -0.3 V chosen from the Fig. 7 in 3 mol dm^{-3} NaOH and 1.2 mol dm^{-3} H$_2$O$_2$. As seen from Fig. 10, the reduction densities steady at around -140, -110, -75 and -30 mA cm^{-2}, respectively, when the potentials are fixed at -0.6, -0.5, -0.4 and -0.3 V. Super current density will be achieved high applied potential, which can be ascribed to the drive force and fast kinetics at noble potential, similar results can be seen from some previous reports [21, 50]. Although some oxygen gas was produced from the hydrolysis of H$_2$O$_2$ on the MnO$_2$/C@TiO$_2$ surface [51], there isn't anything falling from the electrode during the whole reaction process, demonstrating that MnO$_2$/C@TiO$_2$ is stable and equal to fuel cell system.

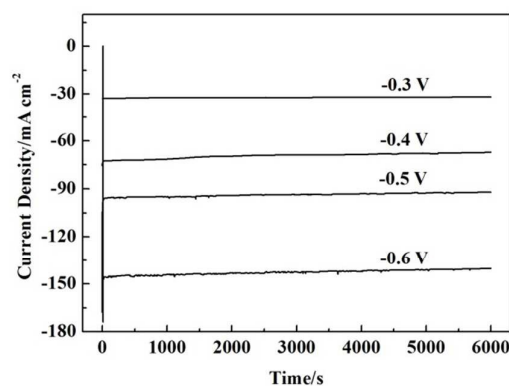Fig. 10 CAs of MnO$_2$/C@TiO$_2$ (60 min) in 3 NaOH mol dm^{-3} +1.2 mol dm^{-3} H$_2$O$_2$ at different potential (-0.6~-0.3 V).

Conclusions

In this paper, MnO$_2$ was demonstrated to be an effectively catalyst for H$_2$O$_2$ electroreduction that atomic oxygen in H$_2$O$_2$ is reduced on the MnO$_2$ surface accompanied with the transformation of Mn^{3+} and Mn^{4+}, and the MnO$_2$/C@TiO$_2$ owns high electrocatalytic activity and super stability in a H$_2$O$_2$ contained alkaline solution. In consideration of the advantages, MnO$_2$/C@TiO$_2$ can be appreciable to reduce the cost and goes into service for FCs.

Acknowledgements

Notes and references

1   O.Z. Sharaf, M.F. Orhan, Renewable Sustainable Energy Rev., 2014, **32**, 810-853.
2   M.R. von Spakovsky, B. Olsommer, Energy Convers. Manage., 2002, **43**, 1249-1257.
3   P. Pei, H. Chen, Appl. Energy, 2014, **125**, 60-75.
4   E. Hollax, J. Power Sources, 1979, **4**, 11-19.
5   N.-C. Shih, B.-J. Weng, J.-Y. Lee, Y.-C. Hsiao, Int. J. Hydrogen Energy, 2014, **39**, 13894-13901.
6   H. Zhao, A. Burke, John Wiley & Sons, Ltd, 2014.
7   D.J. Brodrecht, J.J. Rusek, Appl. Energy, 2003, **74**, 113-124.
8   M.G. Medeiros, R.R. Bessette, C.M. Deschenes, C.J. Patrissi, L.G. Carreiro, S.P. Tucker, D.W. Atwater, J. Power Sources, 2004, **136**, 226-231.
9   N.A. Choudhury, R.K. Raman, S. Sampath, A.K. Shukla, J. Power Sources, 2005, **143**, 1-8.
10 G. Selvarani, S.K. Prashant, A.K. Sahu, P. Sridhar, S. Pitchumani, A.K. Shukla, J. Power Sources, 2008, **178**, 86-91.
11 F. Pei, Y. Wang, X. Wang, P. He, Q. Chen, X. Wang, H. Wang, L. Yi, J. Guo, Int. J. Hydrogen Energy, 2010, **35**, 8136-8142.
12 P. He, Y. Wang, X. Wang, F. Pei, H. Wang, L. Liu, L. Yi, J. Power Sources, 2011, **196**, 1042-1047.
13 R. K. Raman, S. K. Prashant and A. K. Shukla, J. Power Sources, 2006, 162, 1073-1076.
14 D. M. F. Santos, T. F. B. Gomes, B. Šljukić, N. Sousa, C. A. C. Sequeira and F. M. L. Figueiredo, Electrochim. Acta, 2015, 178, 163-170.
15 S.-i. Yamazaki, Z. Siroma, H. Senoh, T. Ioroi, N. Fujiwara, K. Yasuda, J. Power Sources, 2008, **178**, 20-25.
16 A.E. Sanli, A. Aytaç, Int. J. Hydrogen Energy, 36 (2011) 869-875.
17 D.N. Prater, J.J. Rusek, Appl. Energy, 2003, **74**, 135-140.
18 T. Bewer, T. Beckmann, H. Dohle, J. Mergel, D. Stolten, J. Power Sources, 2004, **125**, 1-9.
19 J.-M. You, D. Kim, S. Jeon, Electrochim. Acta, 2012, **65**, 288-293.
20 A. L. Morais, J. R. C. Salgado, B. Šljukić, D. M. F. Santos and C. A. C. Sequeira, Int. J. Hydrogen Energy, 2012, 37, 14143-14151.
21 D. Zhang, K. Ye, D. Cao, J. Yin, K. Cheng, B. Wang, Y. Xu, G. Wang, J. Power Sources, 2015, **273**, 1142-1147.
22 M. Li, S. Xu, M. Tang, L. Liu, F. Gao, Y. Wang, Electrochim. Acta, 2011, **56**, 1144-1149.
23 R.K. Raman, A.K. Shukla, J. Appl. Electrochem., 2005, **35**, 1157-1161.
24 R. Jiang, S. Dong, Electrochim. Acta, 1990, **35**, 1227-1232.
25 H. Liu, L. Zhang, J. Zhang, D. Ghosh, J. Jung, B.W. Downing, E. Whittemore, J. Power Sources, 2006, **161**, 743-752.
26 Y. Li, D. Cao, Y. Liu, R. Liu, F. Yang, J. Yin, G. Wang, Int. J. Hydrogen Energy, 2012, **37**, 13611-13615.
27 D. Cao, J. Chao, L. Sun, G. Wang, J. Power Sources, 2008, **179**, 87-91.
28 G. Wang, D. Cao, C. Yin, Y. Gao, J. Yin, L. Cheng, Chem. Mater., 2009, **21**, 5112-5118.
29 K. Cheng, F. Yang, G. Wang, J. Yin, D. Cao, J. Mater. Chem. A, 2013, **1**, 1669-1676.
30 X. Xiao, F. Yang, K. Cheng, X. Wang, J. Yin, K. Ye, G. Wang, D. Cao, J. Electroanal. Chem., 2014, **729**, 103-108.
31 W. Jia, M. Guo, Z. Zheng, T. Yu, E.G. Rodriguez, Y. Wang, Y. Lei, J. Electroanal. Chem., 2009, **625**, 27-32.
32 L. Zhang, Y. Ni, X. Wang, G. Zhao, Talanta, 2010, **82**, 196-201.
33 F. Cheng, J. Shen, W. Ji, Z. Tao, J. Chen, ACS Appl. Mater. Interfaces, 2009, **1**, 460-466.
34 Y. Ma, R. Wang, H. Wang, J. Key, S. Ji, J. Power Sources, 2015, **280**, 526-532.
35 I. Roche, E. Chaînet, M. Chatenet, J. Vondrák, J. Phys. Chem. C, 2007, **111**, 1434-1443.
36 K.N. Zhu, H.Y. Qin, B.H. Liu, Z.P. Li, J. Power Sources, 2011, **196**, 182-185.
37 D. Duan, S. Liu, C. Yang, Z. Zhang, X. Hao, G. Wei, Y. Li, Int. J. Hydrogen Energy, 2013, **38**, 14261-14268.
38 H. Yang, J. Zhang, S. Kumar, H. Zhang, R. Yang, J. Fang, S. Zou, Electrochem. Commun., 2009, **11**, 2278-2281.
39 W. Weng, C.J. Barile, P. Du, A. Abouimrane, R.S. Assary, A.A. Gewirth, L.A. Curtiss, K. Amine, Electrochim. Acta, 2014, **119**, 138-143.
40 K. Zhang, X. Han, Z. Hu, X. Zhang, Z. Tao, J. Chen, Chem. Soc. Rev., 2015, **44**, 699-728.
41 Q. Zhu, H. Hu, G. Li, C. Zhu, Y. Yu, Electrochim. Acta, 2015, **156**, 252-260.
42 SainanYang, K. Cheng, J. Huang, K. Ye, Y. Xu, D. Cao, X.Z.G. Wang, Electrochim. Acta, 2014, **120**, 416-422.
43 X. Lu, D. Zheng, T. Zhai, Z. Liu, Y. Huang, S. Xie, Y. Tong, , Energy Environ. Sci., 2011, **4**, 2915-2921.
44 S. Khilari, S. Pandit, M.M. Ghangrekar, D. Das, D. Pradhan, RSC Adv., 2013, **3**, 7902-7911.
45 P. Yue, Z. Li, S. Wang, Y. Wang, Int. J. Hydrogen Energy, 2015, **40**, 6809-6817.
46 J. Wu, Q. Wang, A. Umar, S. Sun, L. Huang, J. Wang, Y. Gao, New J. Chem., 2014, **38**, 4420-4426.
47 P. Zhang, D. Guo, Q. Li, Mater. Lett., 2014, **125**, 202-205.
48 K. Huo, X. Zhang, L. Hu, X. Sun, J. Fu, P.K. Chu, Appl. Phys. Lett., 2008, **93**, 013105.
49 W. Zhang, H. Wang, Z. Yang, F. Wang, "Colloids Surf., A", 2007, **304**, 60-66.
50 R. Ding, L. Qi, M. Jia, H. Wang, Electrochim. Acta, 2013, **113**, 290-301.
51 J.J. Dolhun, J. Chem. Educ., 2014, **91**, 760-762.